

CD44-Targeted and Enzyme-Responsive Photo-Cross-Linked Nanogels with Enhanced Stability for In Vivo Protein Delivery

Hong Yu Yang,^{*,||} Jia Meng Du,^{||} Moon-Sun Jang,^{||} Xin Wang Mo, Xin Shun Sun, Doo Sung Lee, Jung Hee Lee,^{*} and Yan Fu^{*}



Cite This: *Biomacromolecules* 2021, 22, 3590–3600



Read Online

ACCESS |



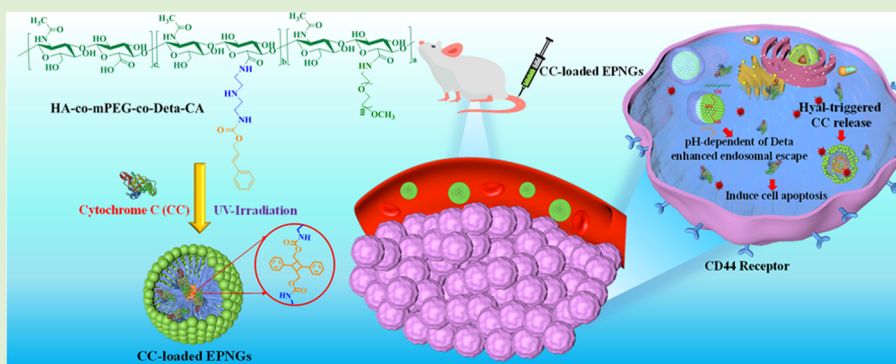
Metrics & More



Article Recommendations



Supporting Information



ABSTRACT: One of the biggest challenges of the protein delivery system is to realize stable and high protein encapsulation efficiency in blood circulation and rapid release of protein in the targeted tumor cells. To overcome these hurdles, we fabricated enzyme-responsive photo-cross-linked nanogels (EPNGs) through UV-triggered chemical cross-linking of cinnamyloxy groups in the side chain of PEGylation hyaluronic acid (HA) for CD44-targeted transport of cytochrome *c* (CC). The EPNGs showed high loading efficiency and excellent stability in different biological media. Notably, CC leakage effectively suppressed under physiological conditions but accelerated release in the presence of hyaluronidase, an overexpressed enzyme in tumor cells. Moreover, thiazolylblue tetrazolium bromide (MTT) results indicated that the vacant EPNGs showed excellent nontoxicity, while CC-loaded EPNGs exhibited higher killing efficiency to CD44-positive A549 cells than to CD44-negative HepG2 cells and free CC. Confocal images confirmed that CC-loaded EPNGs could effectively be internalized by CD44-mediated endocytosis pathway and rapidly escape from the endo/lysosomal compartment. Human lung tumor-bearing mice imaging assays further revealed that CC-loaded EPNGs actively target tumor locations. Remarkably, CC-loaded EPNGs also exhibited enhanced antitumor activity with negligible systemic toxicity. These results implied that these EPNGs have appeared as stable and promising nanocarriers for tumor-targeting protein delivery.

1. INTRODUCTION

A growing number of protein therapeutics progressed, which have been widely used in advanced clinical testing for treating various severe human diseases such as malignant tumors and diabetes mellitus.^{1,2} However, protein-based therapeutics currently only perform extracellular functions for clinical translation, such as monoclonal antibodies and cytokines, while protein drugs have limited intracellular antitumor activities due to their enzymatic degradation, short plasma half-life, and inferior permeability.^{3–5} Therefore, design and development of smart nanocarriers for efficient delivery of proteins to the targeted tumor cells and triggered intracellular liberation of cargos is vital to cancer therapy.⁶

To overcome the above limitations, various protein delivery systems have been developed, including polymeric micelles,^{7–9} nanogels,^{10,11} hydrogels,^{12,13} and liposomes,^{14,15} which provided a promising strategy for reducing immunogenicity and

improving permeability and stability. Particularly, nanogels possess an inner hydrated region for effective protein loading and a hydrophilic outer shell for controlling enzymatic degradation of proteins and inhibiting serum-triggered aggregation of proteins that have captured considerable attention as protein nanocarriers.^{16–18} Moreover, the nanogels with suitable size can not only prolong the circulation time in blood but also be favorably accumulated into tumor sites via the enhanced permeability and retention (EPR) effect.^{19,20} These features enable nanogels to be promising candidates for protein

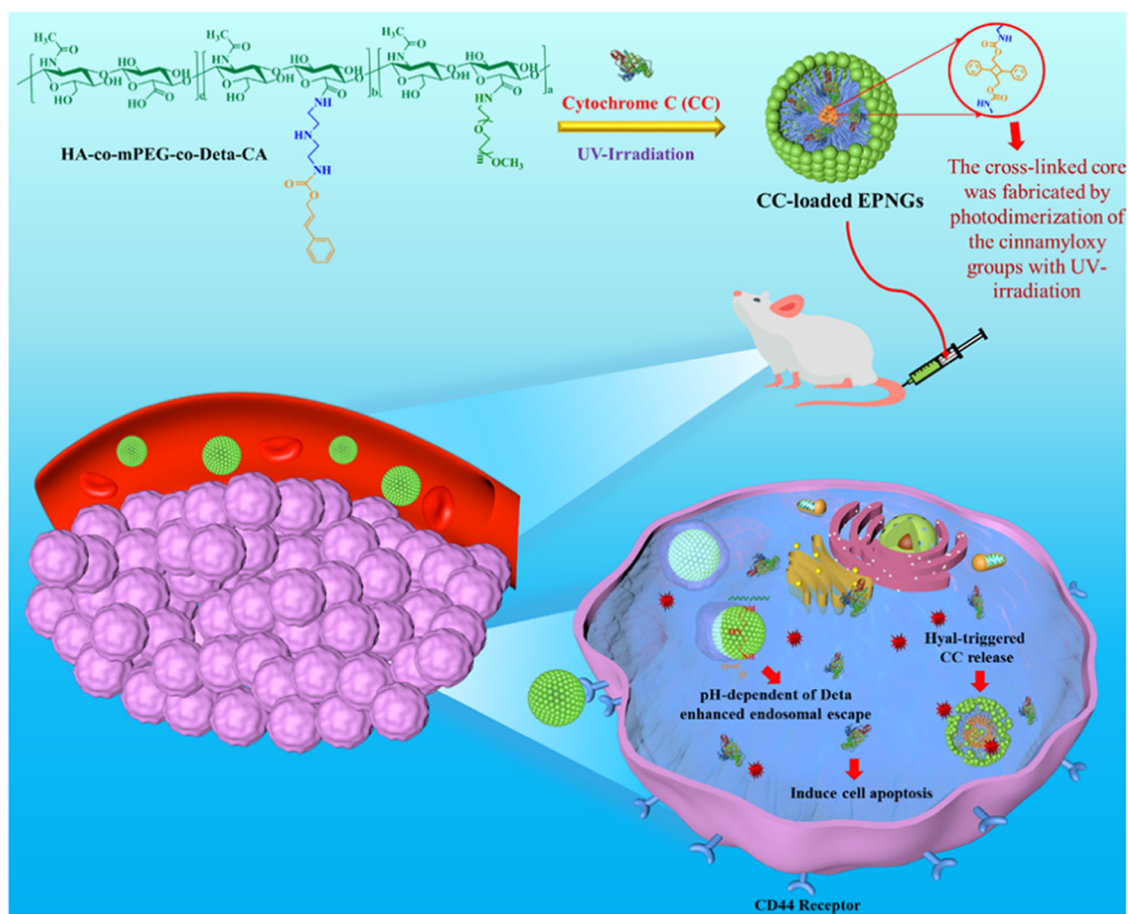
Received: May 24, 2021

Revised: July 7, 2021

Published: July 21, 2021



Scheme 1. Schematic Illustration of Enzyme-Responsive Photo-Cross-Linked Nanogels (EPNGs) for High Loading Efficiency and CD44-Targeted Delivery of CC in A549 Human Lung Tumor-Bearing Nude Mice^a



^aFirst, CC was loaded into the nanoparticles by multiphysical interactions with the HA-co-mPEG-co-Deta-CA polymer and was successfully cross-linked by UV irradiation, which ensured excellent stability of the delivery nanosystems. Second, upon intravenous injection and cellular uptake, CC-loaded EPNGs could effectively be internalized through CD44-mediated endocytosis and subsequent endo-lysosomal escape induced by the “pH-dependent” effect of the Deta-containing polymer. Finally, Hyal-1 enzyme initiated the degradation of HA shells to release CC into cytosolic location and caused cancer cell apoptosis.

delivery in cancer treatment. For example, Zhong et al. constructed EGFR and CD44 dual-targeted nanogels, which were used for the delivery of Granzyme B to breast cancers in vitro and in vivo, leading to an enhanced curative efficacy.²¹ Chen and co-workers designed a hypoxia-responsive nanogel through host–guest interactions between azobenzene and β -cyclodextrin, which was applied to deliver Ribonuclease A and trigger the release of proteins in 4T1 cells, achieving strong therapeutic efficiency in vitro and in vivo.²² We recently also fabricated pH-sensitive and CD44-targeted nanogels by forming acid-labile cross-linked core that accomplished intracellular-triggered release of CC to effectively induce apoptosis of MCF-7 cancer cells.²³

However, there are multiple technical issues that must be addressed in the designing and engineering of nanogels for systemic and cytosolic delivery of proteins. One critical hurdle is related to the stability of nanogels. Because the poor stability of nanogels can easily result in premature protein release in blood circulation, leading to serious side effects and reducing therapeutic efficiency.^{24,25} The second key problem is that nanogels should be able to overcome both extracellular and intracellular obstacles, including tumor-targeting capacity, fast cellular internalization, effective endosomal escape, and

controlled protein release, which are critical for targeted and cytosolic protein delivery.^{26,27} Furthermore, materials based on the fabrication of the nanogels should be rapidly degraded after completing protein delivery.^{28,29} By far, in response to these challenges, many efforts have been devoted to this area, but most can only resolve individual hurdles rather than cover all of the issues.^{30,31} Thus, an effective strategy to tackle the above-mentioned challenges in the systemic and cytosolic delivery of proteins is still rare.

To construct an ideal nanogel, a multifunctional PEGylated hyaluronic acid, HA-co-mPEG-co-Deta-CA (Scheme 1), was prepared. The HA backbone acts as an active tumor-targeting polymer with high-binding affinity to CD44-overexpressed cancer cells.^{32,33} Among its side-chain components, the mPEG segment offers a hydrophilic shell to inhibit nonspecific adsorption to serum proteins; the conjugated Deta components can improve the loading efficiency with proteins and promote endo-lysosomal escape of nanogels into the cytosol based on the pH-dependent protonation of Deta components in the nanogels to disrupt endo/lysosomal membrane (Scheme 1);^{34,35} the pendent cinnamoyloxy groups can form a stable cross-linked core by UV-induced photodimerization reaction (Scheme 1).³⁶ Based on this material, we fabricated enzyme-

responsive photo-cross-linked nanogels (EPNGs) for targeted delivery of cytochrome *c* (CC) as an apoptotic model protein, to the cytosol of cancer cells (Scheme 1). Moreover, our results confirmed that EPNGs displayed excellent stability and high protein-loading efficiency. The resulting CC-loaded EPNGs not only be uptaken via the CD44-mediated endocytic pathway but also rapidly escaped from endo/lysosomal compartment. Notably, CC-loaded EPNGs could also actively target CD44-overexpressed A549 human lung tumors in nude mice and significantly suppressed tumor growth compared to free CC. Overall, this EPNG that incorporates multiple features into a single nanoplatform can overcome numerous challenges for systemic and cytosolic delivery of proteins.

2. EXPERIMENTAL METHOD

2.1. Materials. Sodium hyaluronic acid (HA, $M_n = 9100$ g/mol, degree of polymerization (DP): ~ 23) was obtained from Freda Biopharm Co., Ltd. (Shandong, China). Cinnamyl alcohol (CA), phosphate-buffered saline (PBS), deuterium oxide (D_2O), anhydrous dimethyl sulfoxide (DMSO), cytochrome *c* (CC), dimethyl sulfoxide- d_6 (DMSO- d_6), thiazolylblue tetrazolium bromide (MTT), fetal bovine serum (FBS), 2,2'-azino-bis(3-ethylbenzthiazoline-6-sulfonic acid) (ABTS), Dulbecco's phosphate-buffered saline, RPMI-1640 medium, and pyridine were purchased from Sigma-Aldrich Co., Ltd. (Missouri). *N*-Hydroxysuccinimide (NHS), *N*-(3-dimethylamino-propyl)-*N*-ethylcarbodiimide hydrochloride (EDC), diethylenetriamine (Deta), isothiocyanate isomer (FITC), and hyaluronidase (Hyal-1, 240 N.F.U./mg) were purchased from TCI Co., Ltd. (Tokyo, Japan). Monomethoxy PEG amine (mPEG-NH₂, $M_n = 5000$ Da) was purchased from Ponsure Biological Co., Ltd. (Shanghai, China). 4-Nitrophenyl chloroformate was purchased from Energy Chemical Co., Ltd. (Shanghai, China). LysoTracker Red was purchased from Thermo Fisher Co., Ltd. (Shanghai, China). Cyanine5 (Cy5) NHS ester was purchased from Lumiprobe Co., Ltd. Cy5-CC and FITC-CC were prepared according to our previous research.⁸

2.2. Preparation of HA-co-mPEG-co-Deta-CA. First, Deta-conjugated PEGylated hyaluronic acid, HA-co-mPEG-co-Deta, was synthesized via the amidation reaction with EDC/NHS as the coupling agent. Briefly, HA (1 g, 0.11 mmol) was dissolved in 10 mL of deionized (DI) water in a three-neck flask, then EDC (0.387 g, 2.02 mmol) and NHS (0.233 g, 2.02 mmol) were added to the solution for activating 80% carboxylic groups of HA. The reaction was stirred for 2 h at room temperature (RT) under nitrogen atmosphere (N₂). After activation, mPEG-NH₂ (1.10 g, 0.22 mmol) dispersed in DI water (10 mL) was injected and allowed to unceasingly react for 12 h. Afterward, the aforementioned solution was added dropwise to the stirred solution of DI water (20 mL) containing Deta (3.75 g, 36.4 mmol, 18 times molar to repeating unit of HA) and permitted to further react under the same conditions for 12 h. HA-co-mPEG-co-Deta intermediate polymer was obtained through twice dialysis (MWCO 7000-8000) with DI water followed by freeze-drying. Yield: 93%. Furthermore, cinnamyl alcohol (CA) was conjugated to the HA-co-mPEG-co-Deta by activating the hydroxyl group of CA with 4-nitrophenyl chloroformate (*p*-NPC). In brief, the DMOS solution containing CA (61.5 mg, 0.46 mmol) and pyridine (0.15 mL) was added to the prepared *p*-NPC (92.1 mg, 0.46 mmol) solution in DMSO (5 mL) within 30 min at 0 °C and allowed to react without interruption at RT for 24 h in the dark under N₂. Subsequently, HA-co-mPEG-co-Deta (300 mg, 0.014 mmol) in DI water (10 mL) was added drop by drop to the above mixture solution and allowed to further react by employing the same reaction conditions. The final HA-co-mPEG-co-Deta-CA was collected by dialysis against excess DI water and lyophilization. Yield: 91%. (¹H NMR, 500 MHz, D₂O)

2.3. Preparation of Enzyme-Responsive Photo-Cross-Linked Nanogels (EPNGs). EPNG nanogels were constructed by chemical cross-linking of the cinnamyl groups in the HA-co-mPEG-co-Deta-CA. In brief, HA-co-mPEG-co-Deta-CA polymer was dissolved in phosphate-buffered saline (PBS, 10 mM, pH 7.4), where the polymer

concentration was fixed at 50 mg/mL. The chemical cross-linking of cinnamyl groups was irradiated using a Spectronics XL-1000 equipped with an 8 W lamp for 1 h. The power of light was 40 mW/cm² at 254 nm. To confirm the formation and stability of EPNGs, non-cross-linked polymeric micelles (NLPMs) were prepared by the dialysis method. HA-co-mPEG-co-Deta-CA polymer (50 mg) was completely dissolved in 5 mL of DMSO; then, 20 mL of PBS (10 mM, pH 7.4) was added dropwise under constant stirring. The resulting solution was dialyzed against PBS (pH 7.4) for 24 h to yield the NLPMs. Moreover, the particle sizes of EPNGs and NLPMs in organic solvent were further analyzed to assess the formation of EPNGs with a Zetasizer ZS90 dynamic light scattering (DLS) device. The biological stability of EPNGs and NLPMs was assessed using DLS by dilution in Dulbecco's modified Eagle's medium (DMEM) supplemented with 10% FBS.

2.4. Loading and Release of Protein. Briefly, CC or Cy5-CC was dissolved in 10 mL of PBS (10 mM, pH 7.4) containing various amounts of HA-co-mPEG-co-Deta-CA at a CC/polymer weight ratio of 2 or 20% and stirred for 2 h. Subsequently, CC or Cy5-CC-loaded EPNGs were prepared like those for the fabrication of empty EPNGs. Notably, the secondary structure of CC was not affected using low-band and high-intensity UV irradiation.³⁷ The resulting solution was extensively dialyzed against PBS (pH 7.4) to remove superfluous proteins using the dialysis membrane with 300 kDa. The CC loading content (CLC) and efficiency (CLE) were estimated by subtracting the unloaded CC from the total amount of CC based on a calibration UV-vis absorbance curve of the specified Cy5-CC concentrations. CLC and CLE were estimated by the following equations

$$\text{CLC}\% = (\text{amount of CC in EPNGs} / \text{amount of polymer and loaded CC}) \times 100\%$$

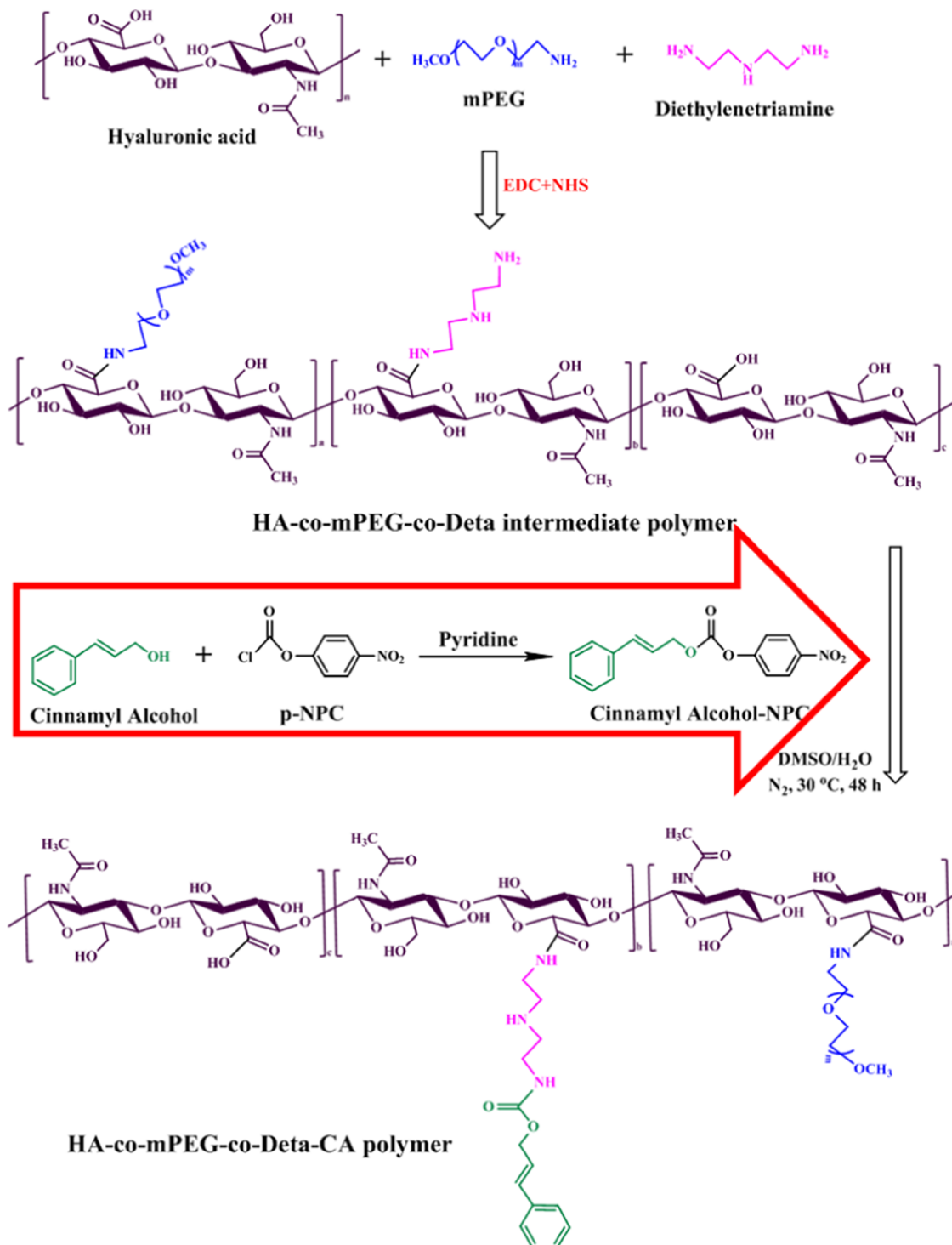
$$\text{CLE}\% = (\text{amount of CC in EPNGs} / \text{total amount of feeding CC}) \times 100\%$$

The release of CC from CC-loaded EPNGs was performed through the dialysis technology. Briefly, a certain number of Cy5-CC-loaded EPNGs were incubated in 5 mL of PBS (pH 7.4) in the presence or absence of 150 U/mL of hyaluronidase^{38,39} and then poured into the dialysis membrane (MWCO = 300 kDa). Subsequently, 3 mL of medium was removed at designated time points and replaced by an equal volume of a new medium. The released mass of CC was estimated by a UV-vis spectrometer (absorption peak at 650 nm).

2.5. Confocal Imaging Assay. The cellular uptake behaviors and endosomal escape capacity of the CC-loaded EPNGs were studied in CD44-positive A549 cells using an LSM700 confocal laser scanning microscope (CLSM, X400, Carl Zeiss) and 2.5 D imaging technology. In brief, A549 cells were treated with Cy5-CC-loaded EPNGs (CC, 20 $\mu\text{g}/\text{mL}$) for 6 h. Then, the cells were washed with PBS thrice and stained using Hoechst 33342 for 10 min. HepG2 cells were selected as a CD44-negative cell model in this study.^{23,40} For the endo/lysosome escape ability assay, A549 cells were treated with FITC-CC-loaded EPNGs in the same control medium for designated time points (2 h and 4 h). Then, the endo/lysosomal compartment was stained with LysoTracker Red probe for 20 min before harvesting the cells, followed by rinsing with PBS three times. The endo/lysosomal escape images of CC-loaded EPNGs were obtained using a CLSM by fixing excitation at 360 nm for Hoechst 33342 ($\lambda_{em} = 460$ nm), 580 nm for LysoTracker ($\lambda_{em} = 590$ nm), and 650 nm for Cy5 ($\lambda_{em} = 670$ nm).

2.6. Evaluation of In Vitro Antitumor Activity. CD44-positive A549 cells and CD44-negative HepG2 cells were seeded at a density of 1×10^4 cells/well in a 96-well plate, which were applied to evaluate the in vitro antitumor activity of CC-loaded EPNGs and free CC using an MTT viability method. Two types of cells were treated with CC-loaded EPNGs or alone CC at various protein concentrations ranging from 5 to 100 $\mu\text{g}/\text{mL}$ and incubated for 24 h. Then, 20 μL of MTT solution in PBS (5 mg/mL) was added and further incubated for 4 h. The supernatant was removed. DMSO (200 μL) was added to each plate to dissolve the generated formazan. The relative cell

Scheme 2. Synthesis Route of the HA-co-mPEG-co-Deta Intermediate Polymer and the HA-co-mPEG-co-Deta-CA Polymer



viability (%) can be determined by comparing the absorbance at 540 nm with a microplate reader. Tests were done in quintuplicate, and data are represented as mean \pm SD. The biocompatibility of blank EPNGs to either A549 or HepG2 cells was studied using the same process at EPNG concentrations ranging from 50 to 500 μ g/mL.

2.7. In Vivo Fluorescence Imaging and Biodistribution Assay. Six-week-old female BALB/c mice (20 ± 2 g) were obtained from Seoul Oriental Bio Center, and experimental processes abided by the guidelines of the Guide for the Care and Use of Laboratory Animals (Institute of Samsung Biomedical of Korea). BALB/c mice were subcutaneously injected in the right flank with A549 cells ($1 \times$

10^7 cells/mouse) to build human lung tumor model. When tumor volumes achieved 100–200 mm³, Cy5-CC-loaded EPNGs (5 mg/kg dose of Cy5-CC) were injected through the tail intravenous administration. Fluorescent scans were monitored at various time intervals (pre, 1, 4, 8, and 24 h) with a near-infrared fluorescence imaging system (IVIS 200, Massachusetts). After 24 h scanning, the mice were sacrificed to isolate tumor and major organs (liver, lung, kidney, heart, and spleen) for evaluation of protein in vivo biodistribution. Moreover, fluorescence intensities of tumor and main organs were further quantified with Living Image 2.5 software (Caliper Life Science).

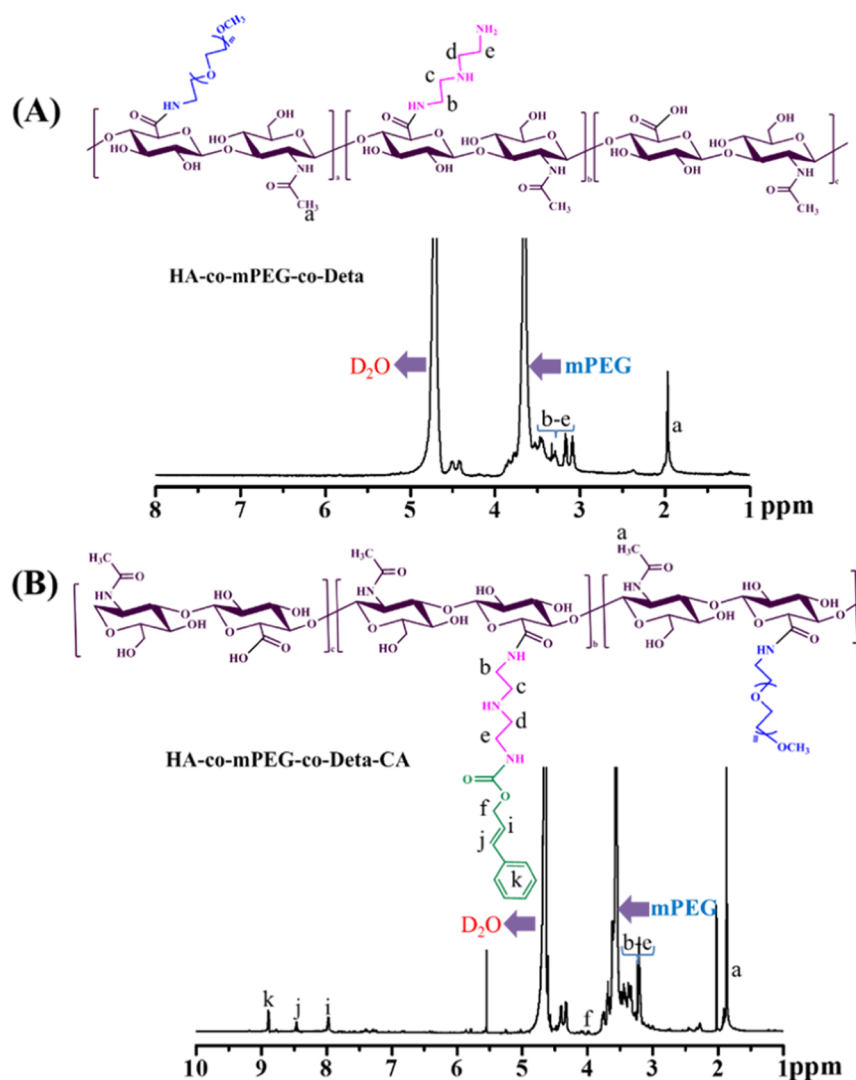


Figure 1. ^1H NMR spectra of the HA-co-mPEG-co-Deta intermediate polymer (A) and the final HA-co-mPEG-co-Deta-CA polymer (B) in D_2O .

2.8. In Vivo Antitumor Efficacy and Biosafe Assessment. A549 tumor-bearing mice were treated with CC-loaded EPNGs or free CC at a dosage of 5 mg of CC equivalents/kg via tail intravenous injection every 3 days when tumor volumes increased to 150–200 mm^3 . Saline was injected as a control group. The tumor volumes and bodyweight of mice were measured every 2 days. Tumor volumes (V) were estimated according to the following formula: $V = (L \times W^2)/2$, where L and W are the tumor length and width, respectively. Relative tumor volumes were estimated as V/V_0 , where V_0 is the initiative tumor volume. Tumor volume, bodyweight, and survival ratios of the mice were monitored every 3 days. The mice were gently killed when the tumor sizes reached approximately 1000 mm^3 . Then, the tumors were removed and weighed. Finally, isolated tumors and main organs (liver, lung, kidney, heart, and spleen) were stained with hematoxylin and eosin (H&E) and TUNEL for histological analysis and biosafety evaluation using a digital microscope.

3. RESULTS AND DISCUSSION

3.1. Synthesis of the HA-co-mPEG-co-Deta-CA Polymer. The HA-co-mPEG-co-Deta-CA polymer was prepared according to a two-step reaction (Scheme 2). For PEGylated HA-co-mPEG-co-Deta polymer, mPEG and Deta were conjugated onto the backbone of HA by amidation reaction using EDC/NHS as coupling agents. Its mPEG ingredient could act as a hydrophilic shell to enhance the stability and

restrain nonspecific adhesion of serum proteins;⁴¹ the Deta was incorporated not only to improve the binding capacity of nanogel to proteins but also to facilitate the escape of nanogels from endo/lysosomal compartments. The successful synthesis of HA-co-mPEG-co-Deta was confirmed using ^1H NMR spectrum (Figure 1A). A distinct characteristic peak at ~ 3.64 ppm associated with the mPEG protons, and the proton peaks ranging from ~ 3.1 to ~ 3.5 ppm, which corresponded to the Deta component in the HA-co-mPEG-co-Deta polymer. For the final HA-co-mPEG-co-Deta-CA polymer, the partially residual amine groups of HA-mPEG-Deta were used to graft the activated CA monomers. By comparing Figure 1A,B, three new proton peaks appeared at ~ 7.9 , ~ 8.4 , and ~ 8.8 ppm, which belonged to the cinnamyloxy groups of the HA-co-mPEG-co-Deta-CA polymer.

The grafting degrees of mPEG, Deta, and CA of the HA-co-mPEG-co-Deta-CA polymer were estimated by integrating the proton signals of each component and the characteristic methyl peaks of acetyl groups of HA, and the detailed results are presented in Table S1.

3.2. Preparation and Properties of EPNGs. Studies about the photodimerization of cinnamyloxy groups to form a cyclobutane ring with low-band UV light have been previously reported.³⁶ Therefore, the EPNGs were easily fabricated by the

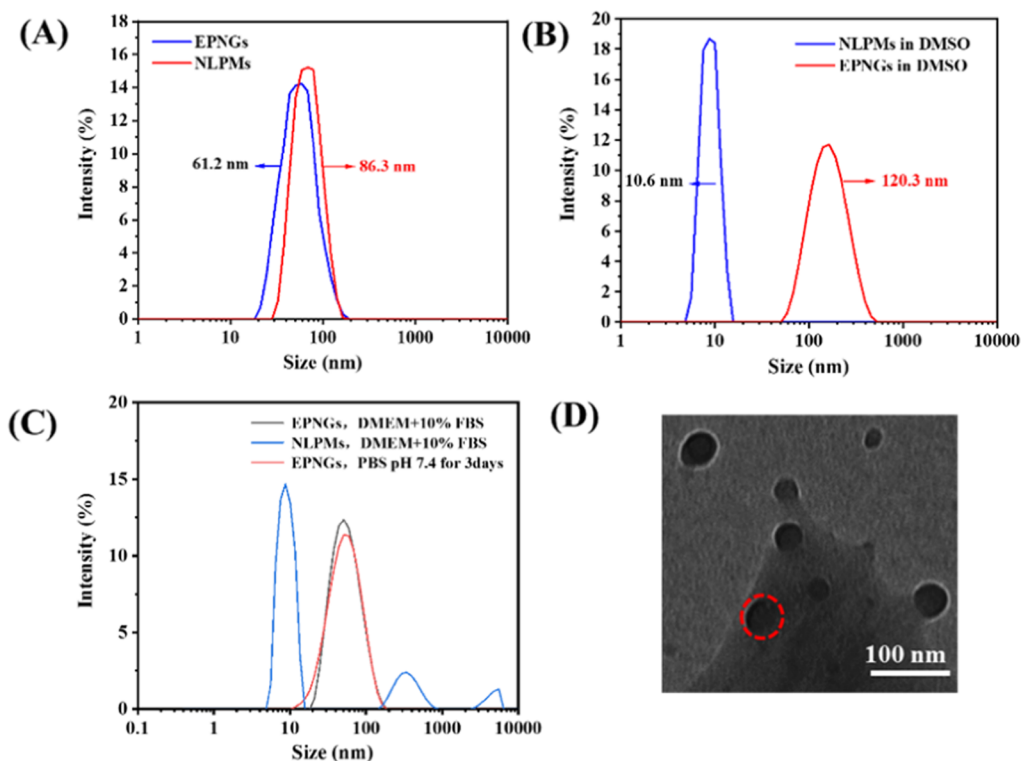


Figure 2. (A) Size distribution of EPNGs and NLPMs. (B) Size change of EPNGs and NLPMs in a large quantity of DMSO solvent. (C) Stability of EPNGs and NLPMs using 100-fold dilutions of DMEM supplement containing 10% FBS and the stability of EPNGs in PBS (pH 7.4) at 37 °C (initial concentration of the sample was set at 1 mg/mL). (D) HR-TEM images of EPNGs.

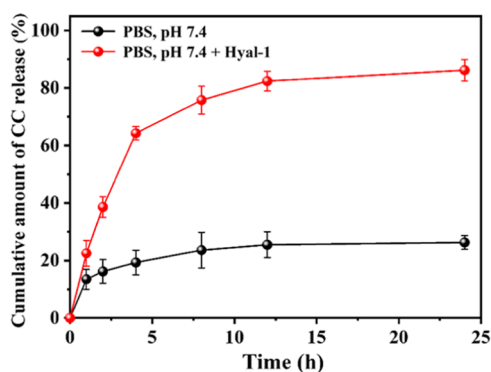


Figure 3. In vitro release of CC from EPNGs incubated in PBS (pH 7.4) with or without Hyal-1 (150 U/mL). Data are presented as mean \pm SD ($n = 3$).

photodimerization of cinnamyloxy groups on the polymer backbone to fabricate a cross-linked core under UV irradiation. To investigate the successful preparation and good stability of EPNGs, non-cross-linked NLPMs as a compared group were fabricated. As shown in Figure 2A, the particle size of EPNGs was about 61 nm, which is smaller than that of the NLPMs. It might be explained that the chemical cross-linking of cinnamyloxy groups further led to the shrinking of nanogels due to enhanced hydrophobic interactions between cinnamyloxy groups to weaken the electrostatic repulsion among residual carboxy groups in the interior of nanoparticles. To further assess the photochemical cross-linking reaction of EPNGs, the EPNGs and NLPMs were, respectively, diluted with the same organic solvent and their particle sizes were evaluated by DLS measurements (Figure 2B). The diameter of

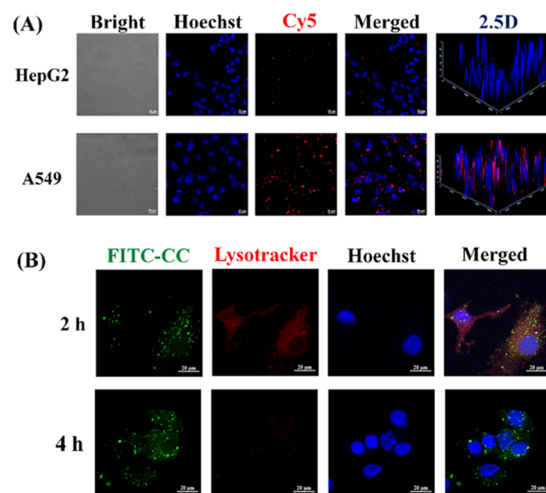


Figure 4. (A) Confocal images and 2.5D images of A549 and HepG2 cells incubated with Cy5-CC-loaded EPNGs for 6 h. (B) Confocal images of A549 cells incubated with FITC-CC-loaded EPNGs for 2 and 4 h, respectively. The cells were counterstained with LysoTracker Red for endo/lysosome and Hoechst for nucleus. The yellow areas indicate colocalization of endolysosome (red) and FITC-CC (green). The scale bars represent 20 μ m.

NLPMs distinctly decreased from the initial \sim 86 to \sim 10 nm by adding a large quantity of DMSO solvent. However, the size of EPNGs increased about 2 times from the original \sim 61 to \sim 120 nm after adding the same amount of solvent. This result indicated that the EPNGs possessed integrated structure through photo-induced cross-linking even after incubating in highly soluble organic solvents. Besides, dilution in a lot of DMEM containing 10% FBS was used to evaluate the stability

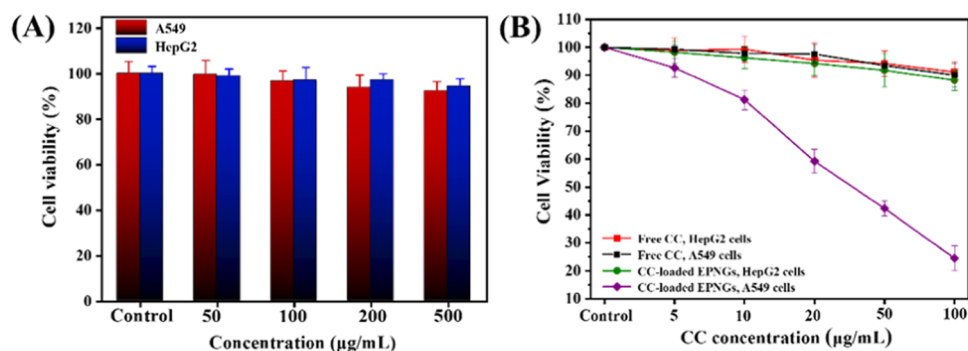


Figure 5. (A) MTT assays of blank EPNGs in A549 and HepG2 cells. (B) MTT assays of CC-loaded EPNGs and free CC in A549 and HepG2 cells ($n = 3$).

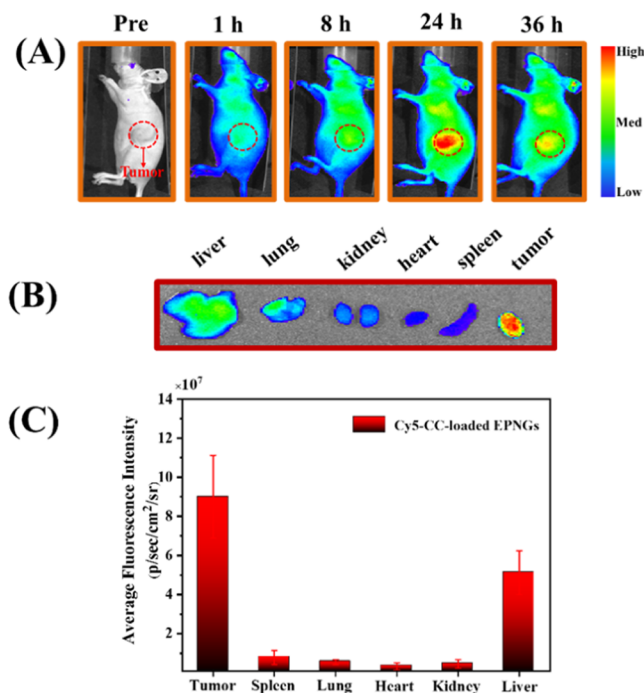


Figure 6. (A) In vivo fluorescence images of A549 human lung tumor-bearing nude mice at different time points following injection of Cy5-CC-loaded EPNGs. Ex vivo fluorescence imaging (B) and the corresponding fluorescence intensities (C) of tumor and main organs isolated at 36 h post-treatment.

of EPNGs mimicking the intravenous injection,⁴² which is essential to apply these nanogels for effective delivery of protein in vivo. As shown in Figure 2C, the NLPs showed partial dissociation against extensive dilution with DMEM containing 10% FBS to the final concentration (~ 0.01 mg/mL) that is lower than the CMC (~ 0.08 mg/mL), as the appearance of multiple peaks. However, the size of EPNGs was almost constant without significant changes under the same diluent condition and in PBS (pH 7.4) for more than 3 days, indicating that these EPNGs containing cross-linked cores significantly improved the stability of nanogels. Moreover, the TEM image in Figure 2D further confirmed that EPNGs exhibited a spherical morphology and particle size distribution close to that the results of DLS assays.

3.3. Loading and Release of CC from EPNGs.

Cytochrome *c* (CC) acted as a protein drug model because the high concentration of CC enables DNA fragmentation in the cell nucleus to induce apoptosis of cancer cells.⁴³ CC could

be effectively encapsulated into EPNGs with a high CLE of 97.8% at a theoretical CLC of 2 wt % and a CLE of 80.3% at a theoretical CLC of 20 wt %. The high loading efficiency of protein is most possibly attributable to the strong multiphysical interactions between CC and HA-co-mPEG-Deta-CA polymers. Moreover, the negative zeta potential of CC-loaded EPNGs slightly decreased from -10.2 to -5.6 mV with increasing CLC from 2 to 20 wt %.

In vitro release patterns of CC from EPNGs were studied with or without hyaluronidase 1 (Hyal-1) conditions. The results in Figure 3 showed that the CC release was significantly suppressed without obvious burst release ($\sim 26\%$ release in 24 h) in a physiological environment (pH 7.4 and 37 °C), while more than 85% of CC was released during 24 h under Hyal-1 condition. The above results not only indicated that the EPNGs with enhanced stability could control the unintended burst release of CC during the blood circulation but also confirmed that the accelerated release of CC could be triggered by Hyal-1, which is an important enzyme in HA degradation and abundant in the cytosol of tumor cells.⁴⁴ Moreover, the 2,2'-azinobis(3-ethylbenzthiazoline-6-sulfonic acid) (ABTS) measurement also confirmed that released CC maintained the same bioactivity as native CC (Figure S1), indicating that CC retained its bioactivity over the CC-loaded EPNG preparation process.

3.4. Confocal Image Analysis and Antitumor Efficacy of CC-Loaded EPNGs In Vitro. CD44-mediated internalization and endo/lysosomal escape capacity of Cy5-CC-loaded EPNGs were evaluated by CLSM in either A549 or HepG2 cells. Confocal images displayed strong Cy5 fluorescence in the cytoplasm of A549 cells after 6 h treatment, indicating efficient cellular uptake of Cy5-CC-loaded EPNGs into A549 cells (Figure 4A). In contrast, a negligible fluorescence signal was found in CD44-negative HepG2 cells after the same incubation time. Notably, the different internalization effects between A549 and HepG2 cells can further be visualized with 2.5D imaging technology without further quantitative analysis (Figure 4A). As expected, meaningless fluorescence signals were observed on both A549 and HepG2 cells with free Cy5-CC after 6 h treatment, indicating that free CC could hardly be uptaken by the tumor cells (Figure S2).⁴⁵ Additionally, exploring the endo/lysosomal escape ability of EPNGs has become one of the key issues for intracellular protein delivery. As shown in Figure 4B, we could clearly observe that the FITC-CC-loaded EPNGs were mainly entrapped in the endo/lysosomal compartments after 2 h incubation, while most CC could successfully escape from the endo/lysosomal compart-

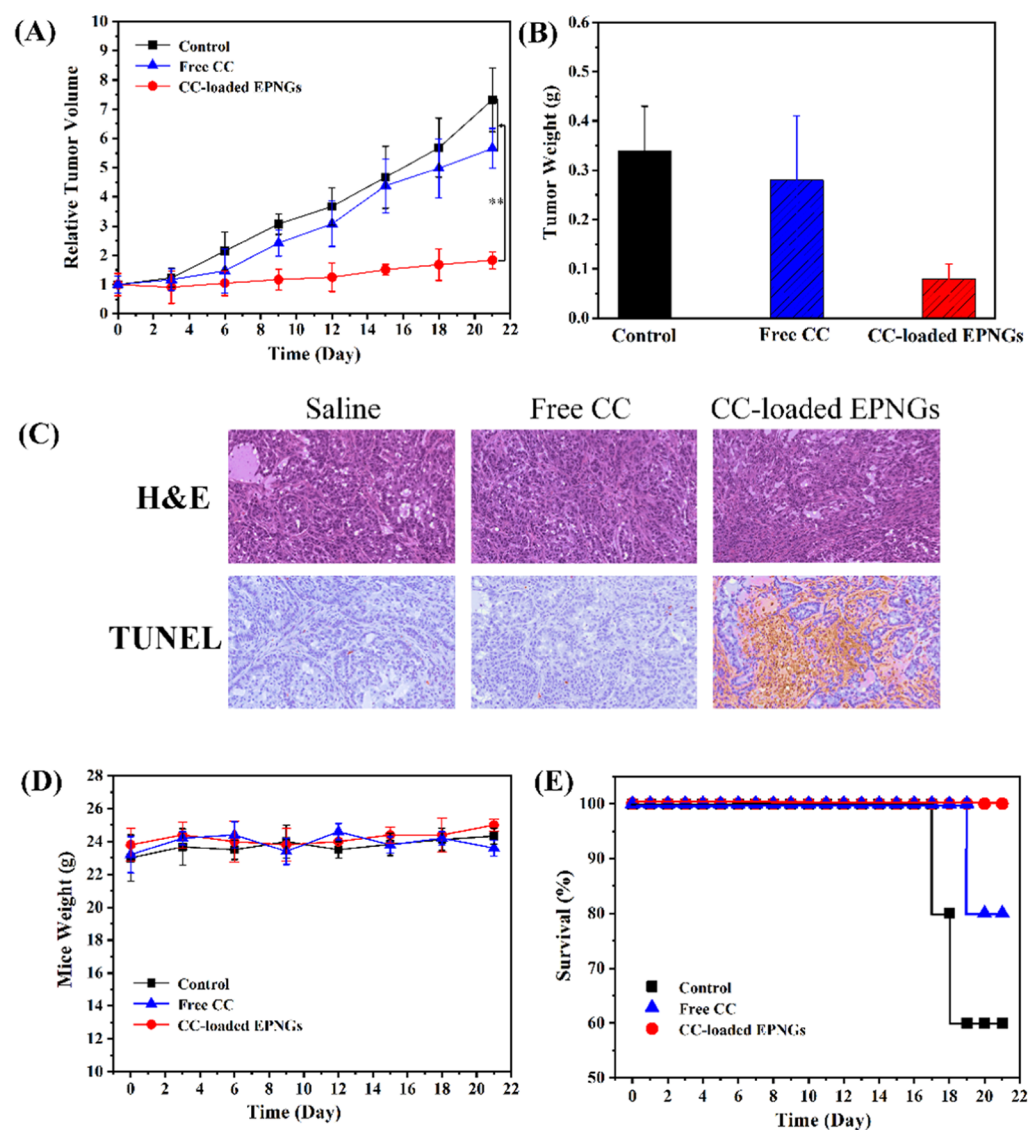


Figure 7. In vivo antitumor efficacy of CC-loaded EPNGs in A549 tumor-bearing nude mice. Free CC and saline groups were used as controls. (A) Changes of relative tumor volumes of A549 tumor-bearing mice after intravenous injection of saline, free CC, and CC-loaded EPNGs within 21 days. ($*p < 0.05$, $**p < 0.01$ using Student's *t*-test). (B) Average weights of isolated tumor sections in three treatment groups on day 21. (C) H&E and TUNEL staining assay of isolated tumor tissues after treatment in different groups. (D) Relative body weights of the mice within 21 days of treatment. (E) Survival rates of the mice in different treatment groups.

ment into the cytoplasm of A549 cells in 4 h. The endo/lysosomal escape ability of CC-loaded EPNGs might be explained that the pH-dependent protonation of Deta components in the EPNGs resulted in destabilization of endo/lysosomal membrane.⁴⁶ It is evident, therefore, that EPNGs exhibited improved cellular internalization and rapid endo/lysosomal escape in CD44-positive A549 cells.

To investigate the cytotoxicity of EPNGs, the cytotoxicity of vacant EPNGs against both A549 and HepG2 cells was evaluated using the standard MTT technology. The cell viability of A549 and HepG2 cells was significantly not changed by treatment with the same concentration of EPNGs ranging from 5 to 500 $\mu\text{g}/\text{mL}$ for 24 h (Figure 5A), indicating that these EPNGs endowed outstanding biocompatibility. The in vitro antitumor efficiency of CC-loaded EPNGs to A549 and HepG2 cells was further assessed by the same procedure. In Figure 5B, free CC as a compared group showed negligible cytotoxicity for each of the cells at various CC concentrations

ranging from 5 to 100 $\mu\text{g}/\text{mL}$, owing mainly to the unaided cellular uptake of free CC. It is worth noting that CD44-positive A549 cells exhibited much better cell apoptosis than CD44-negative HepG2 cells by treatment with CC-loaded EPNGs at an identical CC dose. Negligible cell apoptosis was presented in HepG2 cells treated with the CC-loaded EPNGs because the CC-loaded EPNGs have a negative charge and HepG2 cells act as CD44-negative cancer cells, which led to poor cellular uptake and also supported the results of confocal imaging. Oppositely, these results also further indicated that enhanced cell apoptosis of CC-loaded EPNGs to CD44-overexpressed A549 cells is attributable to the combinative contribution of CD44-mediated endocytosis and the innate endo/lysosomal escape ability of EPNGs.

3.5. In Vivo Targeting and Biodistribution of CC-Loaded EPNGs. In vivo near-infrared fluorescence (NIRF) imaging was performed in A549 tumor xenograft mouse model to evaluate CD44 targetability and biodistribution of Cy5-CC-

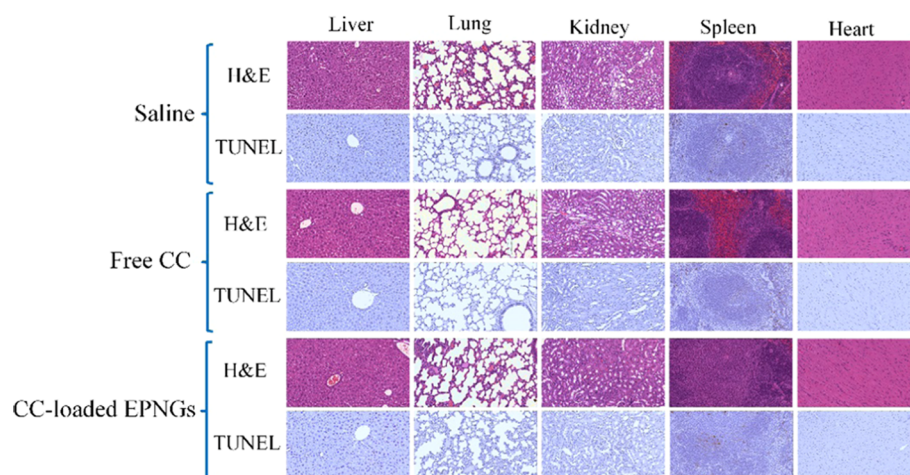


Figure 8. Systemic biosafety assessment. H&E and TUNEL staining of major organs (liver, lung, kidney, spleen, and heart) from the mice bearing A549 lung cancer xenografts treated as described in Figure 7 on day 21.

loaded EPNGs after intravenous injection using a noninvasive imaging system. Figure 6A presents an obvious tumor accumulation effect of Cy5-CC-loaded EPNGs at 8 h post intravenous (i.v.) injection. The strongest fluorescence signal in the tumor site was found at 24 h post-injection. Tumor location fluorescence intensity still remained strong from 24 to 36 h, indicating that Cy5-CC-loaded EPNGs exhibited superior tumor-targeting ability. The NIRF signals in tumor and major organs withdrawn from the A549 tumor-bearing nude mice were detected 36 h after i.v. injection. The fluorescence signal of tumor tissues was significantly higher than those of the liver, spleen, heart, lung, and kidney (Figure 6B), which also agreed with the quantitative results of the ex vivo fluorescence images (Figure 6C). The corresponding high tumor-targeting ability of Cy5-CC-loaded EPNGs is likely attributed to EPR effect-based tumor accumulation, HA-receptor-mediated targeting mechanism, and enhanced stability of the nanosystem.

3.6. In Vivo Antitumor Efficiency and Biosafety Assessment of CC-Loaded EPNGs. Lung cancer remains the leading cause of morbidity and mortality throughout the world.^{47,48} Motivated by their fast internalization, superior endo/lysosomal escape ability, and high tumor accumulation effect, we further assessed the in vivo antitumor efficacy of CC-loaded EPNGs in A549 tumor-bearing mice models. When the volume of tumors reached 150–200 mm³, saline (control group), free CC, and CC-loaded EPNGs were intravenously injected with identical doses of CC (5 mg/kg dose of CC). The results in Figure 7A confirmed that tumor growth was effectively suppressed by treatment with CC-loaded EPNGs during the total treatment period, while rapid tumor progression was detected for control groups receiving saline and free CC. Moreover, these results were supported by the tumor weight withdrawn from the mice after treatment (Figure 7B). At the end of antitumor study, the tumor tissues were stained with the H&E and TUNEL staining to further reveal the highest potency of CC-loaded EPNGs in eradicating A549 tumor cells (Figure 7C). Their biosafety was investigated by monitoring the change in bodyweight and survival rate of mice during the entire treatment period and identifying the histopathological changes of normal organs after treatment. Notably, CC-loaded EPNGs caused little changes in bodyweight and maintained a high survival rate of mice (Figure

7D,E), signifying that these EPNGs had excellent biosafety. Furthermore, the H&E and TUNEL staining assays disclosed that CC-loaded EPNGs caused negligible damage to the major organs, including liver, lung, kidney, spleen, and heart, indicating negligible systemic toxicity (Figure 8). These results suggested that EPNGs are highly effective for protein nanotherapeutics owing to its enhanced stability, which could inhibit unintended protein release during blood circulation and improve their tumor-targeting capacity.

4. CONCLUSIONS

We designed enzyme-responsive photo-cross-linked nanogels (EPNGs) through UV-induced photodimerization of cinnamyl groups. The EPNGs consisting of HA backbone and cross-linked core resulted in enhanced stability and achieved sustained release of CC. They also exhibited fast cellular internalization via CD44-mediated cell adhesion and efficient endo/lysosome escape ability. The CC-loaded EPNGs endowed excellent stability to enable specific targeting of tumor, which was confirmed by the IVIS imaging system. The antitumor ability of CC-loaded EPNGs was better than those of free CC and control groups in vitro and in vivo. Overall, these results demonstrated that the excellent stability of nanogels could markedly impact their tumor-targeting capacity and therapeutic efficiency as protein nanocarriers for use in cancer therapy.

■ ASSOCIATED CONTENT

Supporting Information

The Supporting Information is available free of charge at <https://pubs.acs.org/doi/10.1021/acs.biomac.1c00653>.

Characterization method, assessment of bioactivity of CC released from EPNGs, cell culture method, and 2.5D images of A549 cells and HepG2 incubated with free Cy5-CC (PDF)

■ AUTHOR INFORMATION

Corresponding Authors

Hong Yu Yang – College of Materials Science and Engineering, Jilin Institute of Chemical Technology, Jilin City 132022, P. R. China; orcid.org/0000-0002-0730-2779; Email: yhyqdu@163.com

Jung Hee Lee – Department of Radiology, Samsung Medical Center, Sungkyunkwan University School of Medicine and Center for Molecular and Cellular Imaging, Samsung Biomedical Research Institute, Seoul 06351, Republic of Korea; Email: hijunghee@skku.edu

Yan Fu – College of Materials Science and Engineering, Jilin Institute of Chemical Technology, Jilin City 132022, P. R. China; Email: fuyanqd@163.com

Authors

Jia Meng Du – College of Materials Science and Engineering, Jilin Institute of Chemical Technology, Jilin City 132022, P. R. China

Moon-Sun Jang – Department of Radiology, Samsung Medical Center, Sungkyunkwan University School of Medicine and Center for Molecular and Cellular Imaging, Samsung Biomedical Research Institute, Seoul 06351, Republic of Korea

Xin Wang Mo – College of Materials Science and Engineering, Jilin Institute of Chemical Technology, Jilin City 132022, P. R. China

Xin Shun Sun – College of Materials Science and Engineering, Jilin Institute of Chemical Technology, Jilin City 132022, P. R. China

Doo Sung Lee – Theranostic Macromolecules Research Center and School of Chemical Engineering, Sungkyunkwan University, Suwon, Gyeonggi-do 16419, Republic of Korea;
orcid.org/0000-0002-7979-7459

Complete contact information is available at:

<https://pubs.acs.org/10.1021/acs.biomac.1c00653>

Author Contributions

[†]H.Y.Y., J.M.D., and M.-S.J. contributed equally to this paper.

Notes

The authors declare no competing financial interest.

ACKNOWLEDGMENTS

This research was supported by National Natural Science Foundation of China (NSFC) (no. 21805108) and Outstanding Young Talents Program through a Science and Technology Development Plan Program of Jilin Province (20190103132JH). This research was also supported by the National Research Foundation of Korea (NRF) funded by the Korea government (no. NRF-2020R1A2C2012416).

REFERENCES

- (1) Menacho-Melgar, R.; Decker, J. S.; Hennigan, J. N.; Lynch, M. S. A Review of Lipidation in The Development of Advanced Protein and Peptide Therapeutics. *J. Controlled Release* **2019**, *295*, 1–12.
- (2) He, C.; Tang, Z.; Tian, H.; Chen, X. Co-delivery of Chemotherapeutics and Proteins for Synergistic Therapy. *Adv. Drug Delivery Rev.* **2016**, *98*, 64–76.
- (3) Zhang, P.; Zhang, Y.; Ding, X.; Shen, W.; Li, M.; Wagner, E.; Xiao, C.; Chen, X. A Multistage Cooperative Nanoplatfrom Enables Intracellular Co-Delivery of Proteins and Chemotherapeutics for Cancer Therapy. *Adv. Mater.* **2020**, *32*, No. 2000013.
- (4) Yang, H. Y.; Jang, M. S.; Li, Y.; Lee, J. H.; Lee, D. S. Multifunctional and Redox-Responsive Self-Assembled Magnetic Nanovectors for Protein Delivery and Dual-Modal Imaging. *ACS Appl. Mater. Interfaces* **2017**, *9*, 19184–19192.
- (5) Zhang, Y.; Wu, K.; Sun, H.; Zhang, J.; Yuan, J.; Zhong, Z. Hyaluronic Acid-Shelled Disulfide-Cross-Linked Nanopolymerosomes for Ultrahigh-Efficiency Reactive Encapsulation and CD44-Targeted

Delivery of Mertansine Toxin. *ACS Appl. Mater. Interfaces* **2018**, *10*, 1597–1604.

(6) Wang, X.; Shi, C.; Zhang, L.; Lin, M. Y.; Guo, D.; Wang, L.; Yang, Y.; Duncan, T. M.; Luo, J. Structure-Based Nanocarrier Design for Protein Delivery. *ACS Macro Lett.* **2017**, *6*, 267–271.

(7) Kang, Y.; Lu, L.; Lan, J.; Ding, Y.; Yang, J.; Zhang, Y.; Zhao, Y.; Zhang, T.; Ho, R. Redox-Responsive Polymeric Micelles Formed by Conjugating Gambogic Acid with Bioreducible Poly(amido amine)s for The Co-Delivery of Docetaxel and MMP-9 shRNA. *Acta Biomater.* **2017**, *68*, 137–153.

(8) Sun, X. S.; Jang, M. S.; Fu, Y.; Lee, J. H.; Yang, H. Y.; et al. Intracellular Delivery of Cytochrome C Using Hypoxia-Responsive Polypeptide Micelles for Efficient Cancer Therapy. *Mater. Sci. Eng., C* **2020**, *114*, No. 111069.

(9) Liu, X.; Li, C.; Lv, J.; Huang, F.; Ma, R.; et al. Glucose and H₂O₂ Dual-Responsive Polymeric Micelles for Self-Regulated Release of Insulin. *ACS Appl. Bio Mater.* **2020**, *3*, 1598–1606.

(10) Huang, K.; He, Y.; Zhu, Z.; Guo, J.; Wang, G.; Deng, C.; Zhong, Z. Small, Traceable, Endosome-Disrupting, and Bioresponsive Click Nanogels Fabricated via Microfluidics for CD44-Targeted Cytoplasmic Delivery of Therapeutic Proteins. *ACS Appl. Mater. Interfaces* **2019**, *11*, 22171–22180.

(11) Chen, J.; Ouyang, J.; Chen, Q.; Deng, C.; Meng, F.; Zhang, J.; Cheng, R.; Lan, Q.; Zhong, Z. EGFR and CD44 Dual-Targeted Multifunctional Hyaluronic Acid Nanogels Boost Protein Delivery to Ovarian and Breast Cancers in Vitro and in Vivo. *ACS Appl. Mater. Interfaces* **2017**, *9*, 24140–24147.

(12) Vermonden, T.; Censi, R.; Hennink, W. E. Hydrogels for Protein Delivery. *Chem. Rev.* **2012**, *112*, 2853–2888.

(13) Sim, H. J.; Thambi, T.; Lee, D. S. Heparin-based Temperature-sensitive Injectable Hydrogels for Protein Delivery. *J. Mater. Chem. B* **2015**, *3*, 8892–8901.

(14) Wang, A.; Yang, T.; Fan, W.; Yang, Y.; Zhu, Q.; Guo, S.; Zhu, C.; Yuan, Y.; Zhang, T.; Gan, Y. Protein Corona Liposomes Achieve Efficient Oral Insulin Delivery by Overcoming Mucus and Epithelial Barriers. *Adv. Healthcare Mater.* **2019**, *8*, No. 1801123.

(15) Vila-Caballer, M.; Gaia, C.; Alessio, M.; Stefano, S.; pH-sensitive, A. Stearoyl-PEG-poly(methacryloyl sulfadimethoxine)-Decorated Liposome System for Protein Delivery: An Application for Bladder Cancer Treatment. *J. Controlled Release* **2016**, *238*, 31–42.

(16) Zhu, Q.; Chen, X.; Xu, X.; Zhang, Y.; Zhang, C.; Mo, R. Tumor-Specific Self-Degradable Nanogels as Potential Carriers for Systemic Delivery of Anticancer Proteins. *Adv. Funct. Mater.* **2018**, *28*, No. 1707371.

(17) Hashimoto, Y.; Mukai, S.; Sasaki, Y.; Akiyoshi, K. Nanogel Technics for Tissue Engineering: Protein Delivery Systems with Nanogel Chaperones. *Adv. Healthcare Mater.* **2018**, *7*, No. 1800729.

(18) Yin, Y.; Hu, B.; Yuan, X.; Cai, L.; Gao, H.; Yang, Q. Nanogel: A Versatile Nano-Delivery System for Biomedical Applications. *Pharmaceutics* **2020**, *12*, No. 290.

(19) Kalyane, D.; Raval, N.; Maheshwari, R.; Tambe, V.; Kalia, K.; Tekade, R. K. Employment of Enhanced Permeability and Retention Effect (EPR): Nanoparticle-Based Precision Tools for Targeting of Therapeutic and Diagnostic Agent in Cancer. *Mater. Sci. Eng., C* **2019**, *98*, 1252–1276.

(20) Liu, Y.; Sun, D.; Fan, Q.; Ma, Q.; Wang, C.; et al. The Enhanced Permeability and Retention Effect Based Nanomedicine at The Site of Injury. *Nano Res.* **2020**, *13*, 564–569.

(21) Chen, J.; Ouyang, J.; Chen, Q.; Deng, C.; Meng, F.; Zhang, J.; Cheng, R.; Lan, Q.; Zhong, Z. EGFR and CD44 Dual-Targeted Multifunctional Hyaluronic Acid Nanogels Boost Protein Delivery to Ovarian and Breast Cancers In Vitro and In Vivo. *ACS Appl. Mater. Interfaces* **2017**, *9*, 24140–24147.

(22) Si, X.; Ma, S.; Xu, Y.; Zhang, D.; Shen, N.; Yu, H.; Zhang, Y.; Song, W.; Tang, Z.; Chen, X. Hypoxia-Sensitive Supramolecular Nanogels for the Cytosolic Delivery of Ribonuclease A as A Breast Cancer Therapeutic. *J. Controlled Release* **2020**, *320*, 83–95.

(23) Yang, H. Y.; Yi, L.; Jang, M. S.; Yan, F.; Wu, T. P.; Lee, J. H.; Lee, D. S. Green Preparation of pH-responsive and Dual Targeting

Hyaluronic Acid Nanogels for Efficient Protein Delivery. *Eur. Polym. J.* **2019**, *121*, No. 109342.

(24) González-Toro, D. C.; Ryu, J. H.; Chacko, R. T.; Zhuang, J.; Thayumanavan, S. Concurrent Binding and Delivery of Proteins and Lipophilic Small Molecules Using Polymeric Nanogels. *J. Am. Chem. Soc.* **2012**, *134*, 6964–6967.

(25) Kim, C. S.; Mout, R.; Zhao, Y.; Yeh, Y. C.; Tang, R.; Jeong, Y.; Duncan, B.; Hardy, J. A.; Rotello, V. M. Co-Delivery of Protein and Small Molecule Therapeutics Using Nanoparticle-Stabilized Nanocapsules. *Bioconjugate Chem.* **2015**, *26*, 950–954.

(26) Mura, S.; Nicolas, J.; Couvreur, P. Stimuli-responsive Nanocarriers for Drug Delivery. *Nat. Mater.* **2013**, *12*, 991–1003.

(27) Lv, L.; Fan, Q.; Wang, H.; Cheng, Y. Polymers for Cytosolic Protein Delivery. *Biomaterials* **2019**, *218*, No. 119358.

(28) Saghazadeh, S.; Rinoldi, C.; Schot, M.; Kashaf, S. S.; Khademhosseini, A.; et al. Drug Delivery Systems and Materials for Wound Healing Applications. *Adv. Drug Delivery Rev.* **2018**, *127*, 138–166.

(29) Yau, A.; Lee, J.; Chen, Y. Nanomaterials for Protein Delivery in Anticancer Applications. *Pharmaceutics* **2021**, *13*, No. 155.

(30) Fu, Y.; Jang, M. S.; Wu, T.; Lee, J. H.; Li, Y.; Lee, D. S.; Yang, H. Y. Multifunctional Hyaluronic Acid-Mediated Quantum Dots for Targeted Intracellular Protein Delivery and Real-Time Fluorescence Imaging. *Carbohydr. Polym.* **2019**, *224*, No. 115174.

(31) Srivastava, S.; Sharma, V.; Bhushan, B.; Malviya, R.; Kulkarni, G. T. Nanocarriers for Protein and Peptide Delivery: Recent Advances and Progress. *J. Res. Pharm.* **2021**, *25*, 99–116.

(32) Choi, K. Y.; Yoon, H. Y.; Kim, J. H.; Bae, S. M.; Park, R. W.; Kang, Y. M.; Kim, I. S.; Kwon, I. C.; Choi, K.; Jeong, S. Y.; et al. Smart Nanocarrier Based on PEGylated Hyaluronic Acid for Cancer Therapy. *ACS Nano* **2011**, *5*, 8591–8599.

(33) Li, Y.; Le, T. M. D.; Bui, Q. N. A.; Yang, H. Y.; Lee, D. S. Tumor Acidity and CD44 Dual Targeting Hyaluronic Acid-coated Gold Nanorods for Combined Chemo- and Photothermal Cancer Therapy. *Carbohydr. Polym.* **2019**, *226*, No. 115281.

(34) Kim, H. J.; Ishii, A.; Miyata, K.; Lee, Y.; Wu, S.; Oba, M.; et al. Introduction of Stearoyl Moieties into A Biocompatible Cationic Polyaspartamide Derivative, Pasp (DET), with Endosomal Escaping Function for Enhanced siRNA-Mediated Gene Knockdown. *J. Controlled Release* **2010**, *145*, 141–148.

(35) Miyata, K.; Oba, M.; Nakanishi, M.; Fukushima, S.; Yamasaki, Y.; Koyama, H.; et al. Polyplexes from Poly (aspartamide) Bearing 1, 2-Diaminoethane Side Chains induce pH-Selective, Endosomal Membrane Destabilization with Amplified Transfection and Negligible Cytotoxicity. *J. Am. Chem. Soc.* **2008**, *130*, 16287–16294.

(36) Ding, J.; Zhuang, X.; Xiao, C.; Cheng, Y.; Li, Z.; He, C.; Tang, Z.; Chen, X. Preparation of Photo-Cross-Linked PH-responsive Polypeptide Nanogels as Potential Carriers for Controlled Drug Delivery. *J. Mater. Chem.* **2011**, *21*, 11383–11391.

(37) Chen, J.; Zou, Y.; Deng, C.; Meng, F.; Zhang, J.; Zhang, Z. Multifunctional Click Hyaluronic Acid Nanogels for Targeted Protein Delivery and Effective Cancer Treatment in Vivo. *Chem. Mater.* **2016**, *28*, 8792–8799.

(38) Yoon, H. Y.; Koo, H.; Choi, K. Y.; Lee, S. J.; Kim, K.; Kwon, I. C.; Leary, J. F.; Park, K.; Yuk, S. H.; Park, J. H.; Choi, K. Tumor-Targeting Hyaluronic Acid Nanoparticles for Photodynamic Imaging and Therapy. *Biomaterials* **2012**, *33*, 3980–3989.

(39) Lin, T.; Yuan, A.; Zhao, X.; Lian, H.; Zhuang, J.; Chen, W.; Zhang, Q.; Liu, G.; Zhang, S.; Chen, W.; Cao, W.; Zhang, C.; Wu, J.; Hu, Y.; Guo, H. Self-assembled Tumor-Targeting Hyaluronic Acid Nanoparticles for Photothermal Ablation in Orthotopic Bladder Cancer. *Acta Biomater.* **2017**, *53*, 427–438.

(40) Lin, W. J.; Lee, W. C.; Shieh, M. J. Hyaluronic Acid Conjugated Micelles Possessing CD44 Targeting Potential for Gene Delivery. *Carbohydr. Polym.* **2017**, *155*, 101–108.

(41) Lin, W. J.; Lee, W. C. Polysaccharide-Modified Nanoparticles with Intelligent CD44 Receptor Targeting Ability for Gene Delivery. *Int. J. Nanomed.* **2018**, *13*, 3989.

(42) Chen, J.; Ouyang, J.; Kong, J.; Wen, Z.; Xing, M. Photo-Cross-Linked and pH-Sensitive Biodegradable Micelles for Doxorubicin Delivery. *ACS Appl. Mater. Interfaces* **2013**, *5*, 3108–3117.

(43) Qureshi, M. A.; Khatoon, F. Different Types of Smart Nanogel for Targeted Delivery. *J. Sci.: Adv. Mater. Devices* **2019**, *4*, 201–212.

(44) Yoon, H. Y.; Koo, H.; Choi, K. Y.; Kwon, I. C.; Choi, K.; Park, J. H.; Kim, K. Photo-Crosslinked Hyaluronic Acid Nanoparticles with Improved Stability for in Vivo Tumor-targeted Drug Delivery. *Biomaterials* **2013**, *34*, 5273–5280.

(45) Qiu, M.; Zhang, Z.; Wei, Y.; Sun, H.; Meng, F.; Deng, C.; Zhong, Z. Small-sized and Robust Chimaeric Lipopepsomes: A Simple and Functional Platform with High Protein Loading for Targeted Intracellular Delivery of Protein Toxin in Vivo. *Chem. Mater.* **2018**, *30*, 6831–6838.

(46) Yang, H. Y.; Fu, Y.; Jang, M. S.; Li, Y.; Lee, J. H.; Chae, H.; Lee, D. S. Multifunctional Polymer Ligand Interface CdZnSeS/ZnS Quantum Dot/Cy3-Labeled Protein Pairs as Sensitive FRET Sensors. *ACS Appl. Mater. Interfaces* **2016**, *8*, 35021–35032.

(47) Bade, B. C.; Cruz, C. S. D. Lung cancer 2020: Epidemiology, Etiology, and Prevention. *Clin. Chest Med.* **2020**, *41*, 1–24.

(48) Zhang, L.; Zhu, B.; Zeng, Y.; Shen, H.; Zhang, J.; Wang, X. Clinical Lipidomics in Understanding of Lung Cancer: Opportunity and Challenge. *Cancer Lett.* **2020**, *470*, 75–83.